



Analytical prediction of the axial capacity of concrete-filled cold-formed steel (CF-CFS) built-up columns

Rohola Rahnavard¹, Hélder D. Craveiro², Rui A. Simões³

Abstract

Cold-formed steel (CFS) built-up sections are being increasingly used in the construction sector, especially as compression members. One of the challenges of these compression members is their sensitivity to early buckling under compression. The CFS closed built-up columns can be filled with concrete to overcome the early buckling and to increase its axial load-bearing capacity. As a consequence, the applicability of the design prediction in these sections should be investigated; this is, therefore, the purpose of this paper. First, the results of twenty-four experimental specimens, including four full and partial concrete-filled cold-formed steel (CF-CFS) section configurations with two different lengths under pure compression, are presented. Then, a finite element modelling approach is calibrated against the experimental data, and consequently, a parametric study is used to investigate a larger range of slenderness. Finally, the axial load-bearing capacity of the CF-CFS built-up composite columns is compared to the design predictions according to EN 1994-1-1 and the AISC Specification. Reliability analysis is also performed to assess and compare the available and proposed methodologies. The results show that both standards present an unconservative prediction for the partial CF-CFS columns and a highly conservative for the full CF-CFS composite columns. Therefore, this paper modifies EN 1994-1-1 and the AISC analytical procedures to be applicable in predicting the buckling resistance of the CF-CFS composite columns. The paper first suggests extending the constant range of the buckling curve of EN 1994-1-1 from a non-dimensional slenderness of 0.2 to 0.4, then defines two new buckling curves by proposing two imperfection factors, specifically for the partial and full CF-CFS columns.

Keywords

Axial load-bearing capacity; built-up sections; cold-formed steel; composite column; concrete-filled.

¹ PhD candidate, University of Coimbra, ISISE, Department of Civil Engineering, rahnavard1990@gmail.com; rahnavard@uc.pt

² Lecturer, University of Coimbra, ISISE, Department of Civil Engineering, heldercraveiro.eng@uc.pt

³ Associate professor, University of Coimbra, ISISE, Department of Civil Engineering, rads@dec.uc.pt

1. Introduction

Concrete-filled cold-formed steel (CF-CFS) built-up composite column is a novel composite structural member consisting of a CFS closed built-up section filled with lightweight concrete, exploring the advantageous characteristics of each material. The closed built-up CFS acts as formwork and remains in the structure, avoids the use of other traditional formwork, and saves time. Consequently, it provides a low-cost and more sustainable system. Moreover, closed built-up CFS provides confinement to the concrete infill, leading to a higher axial load-bearing capacity and more suitable compression performance (Rahnavard et al. 2022). Concrete also prevents premature local buckling phenomena on the thin-walled CFS profiles, enhancing their performance under compression.

Due to the high axial capacity and enhanced structural fire performance, composite concrete-filled steel tubular columns are widely used in structures. Several experimental, analytical, and numerical studies have been carried out to investigate the behaviour of concrete-filled steel tubular composite columns under compression (Han et al. 2011, Uy et al. 2011, Hassanein & Kharoob 2014, Hassanein et al. 2015, 2023, Kazemzadeh & Uy 2020). Several design methodologies have also been proposed to predict the buckling resistance of concrete-filled steel tube composite columns by focusing on the effect of provided confinement of steel tubes (Uenaka et al. 2010 and Yan et al. 2021). Moreover, the design of such columns is comprehensively covered in different design codes, including EN 1994-1-1 and the AISC Specification. However, most prior studies focus on the composite column made of standard tubular sections, lacking versatility. At the same time, no research has been conducted to investigate the applicability of the thin-walled CFS built-up sections for composite columns or to determine the applicability of available design methodologies for such types of columns; this is, therefore, the focus of the present study.

The focus was initially placed on presenting the experimental test results, including the axial load-bearing capacities and deformed shapes. A finite element modelling approach was after that validated and the results were calibrated. A parametric study was then conducted to investigate the applicability of the available design methods. Finally, a reliability analysis was conducted to assess further the design methodologies.

2. Experimental study

2.1 Geometry and material property

The objective of this investigation was to assess the compressive behaviour of four innovative CF-CFS configurations, including two rectangular shapes (R-2C+2U and R-2 Σ +2U) and two square shapes (S-2C+2U and S-2 Σ +2U) cross-sections. The test specimens were designed and two lengths considered, namely 1050 mm and 3000 mm aiming to investigate the governing buckling modes, local and interaction between local and global buckling, respectively. Three repetitions were considered for each column to ensure the accuracy of the test results. First, the CFS built-up columns were constructed with four individual CFS profiles and then filled with lightweight concrete. Profiles were fastened using self-drilling screws (with a diameter of 6.3 mm). Fig. 1 shows the individual CFS profiles (C, U, and Σ). All individual profiles have the same thickness of 1.5 mm and are classified as Class-4 cross-sections. According to a preliminary design conducted by Craveiro et al. (2022), the distance between fasteners along the longitudinal direction of the columns was 237.5 mm for the short and 362.5 mm for the long CF-CFS composite columns

ensuring a partial composite action between the individual CFS shapes. Figs. 2 and 3 show the geometry and the CF-CFS columns' experimental specimens, respectively.

The material properties were measured using a set of coupon tests for the CFS (Craveiro et al. 2022) and cubic compression tests for lightweight concrete (Rahnavard et al. 2022). According to the coupon tests, the average modulus of elasticity (E_s) measured was 204 GPa. The average value for the yield stress (f_y) was 306.81 MPa (0.2% proof stress), and for the ultimate stress (f_u) was 424.04 MPa. The mean compressive strength (f_{cm}) and density (D) for the lightweight concrete were obtained as 33 MPa and 1850 kg/m³, respectively.

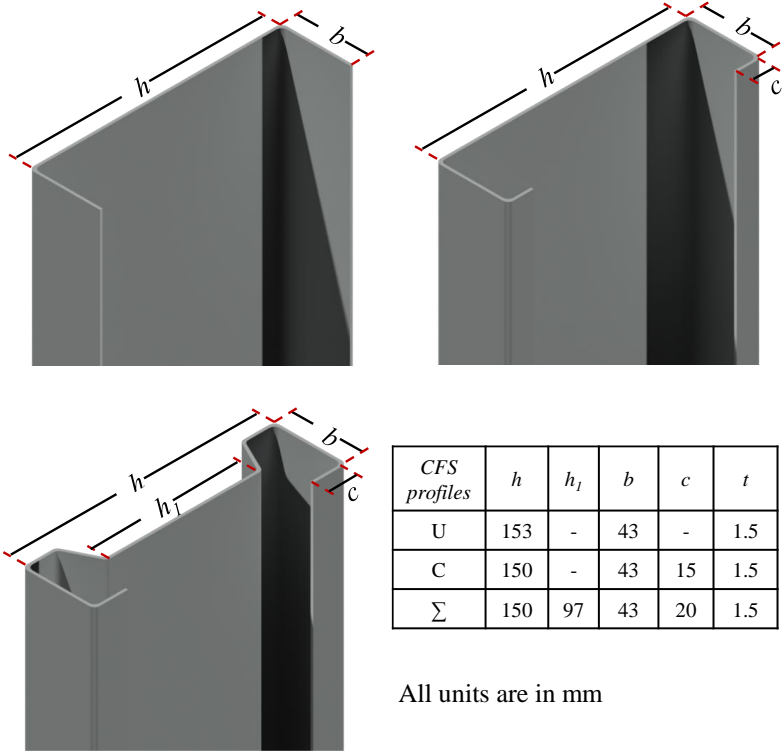


Figure 1: Geometry of CFS profiles

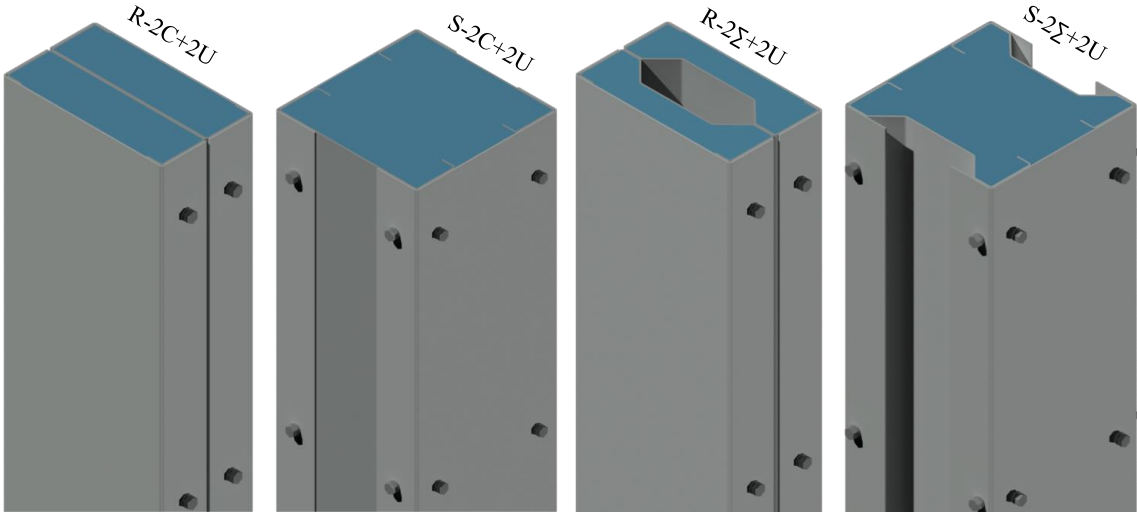


Figure 2: CF-CFS configurations.

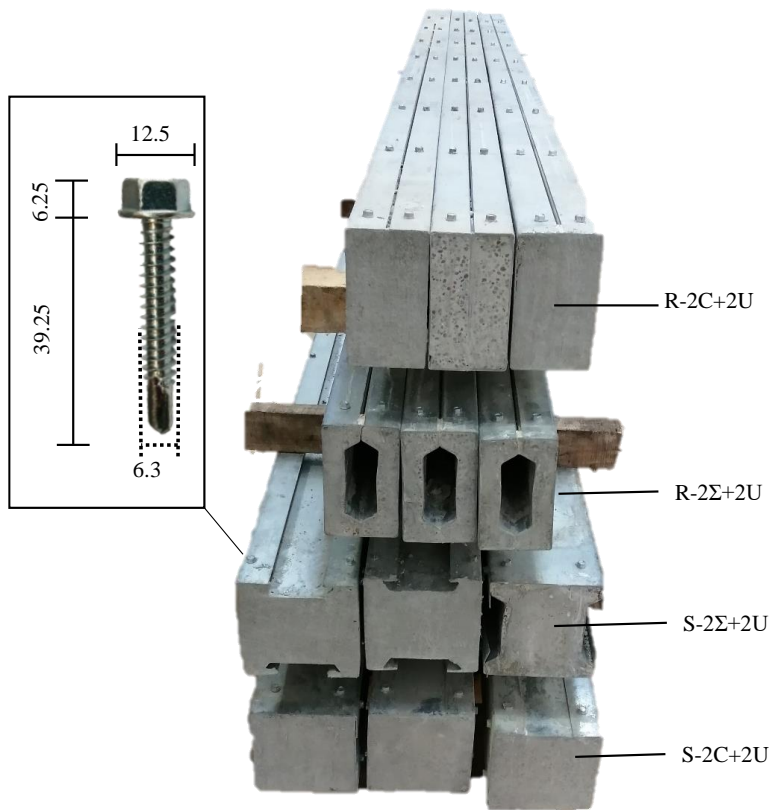


Figure 3: experimental specimens of the long composite columns.

2.2 Test setup

In the experimental investigation, two test setups were considered due to the different lengths of the designed specimens. The short CF-CFS columns were tested using a universal testing machine with a capacity of 5000 kN (Fig. 4a), whereas for the long CF-CFS columns, a reaction frame was used, and a hydraulic jack fixed to it to apply the axial force (Fig. 4b). The columns' ends were fixed against translational and rotational movements (see Fig. 5). Loading was applied under displacement control at a constant rate of 0.01 mm/s. The vertical end-shortening displacement was measured during the test using a 100 mm range Linear Variable Differential transformer (LVDT). The CF-CFS built-up column buckling tests were stopped when clear drops of the axial load were observed.

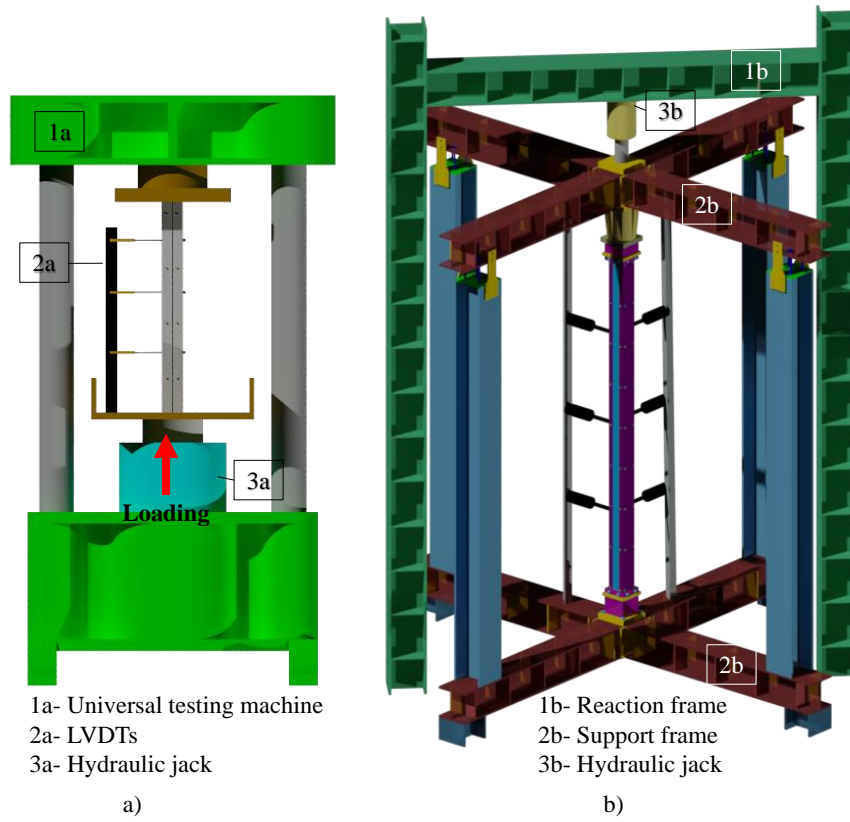


Figure 4: Schematic view of the setup for a) short columns and b) long columns



Figure 5: Test setup detail for a) short columns and b) long columns

3. Numerical modelling

Numerical models were developed to reproduce the observed experimental behaviour using the finite element software Abaqus, contributing to a better understanding of the CF-CFS built-up columns. The CFS material property was defined in the elastoplastic range. The modulus of elasticity and Poisson ratio of 204 GPa and 0.3 were used to define the elastic range, and the true plastic stress-strain curve was used to define the plasticity. Note that the true stress-strain curve was calculated by converting the engineering stress-strain curve, as shown in Fig. 6.

Similarly, the concrete elasticity was defined by considering the modulus of elasticity and Poisson ratio. The modulus of elasticity was calculated according to Eq. 1, suggested by EN 1992-1-1:

$$E_{cm} = 22(f_{cm}/10)^{0.3} \quad (1)$$

where f_{cm} is the mean compressive strength of the concrete. The concrete's compressive strength from the cubic tests was 33 MPa, and the modulus of elasticity obtained was 31.47 GPa. The concrete damage plasticity (CDP) model available in Abaqus was used to define the plastic behaviour of the concrete parts. The plastic compressive and tensile behaviour of concrete is needed to define the CDP model. Fig. 7a shows the compressive stress-strain curve for concrete with a mean strength of 33 MPa. First, the plastic compressive stress-strain curve was plotted using Eq. 2, suggested by EN 1992-1-2, up to the nominal ultimate strain of 0.0035 (OAB) and then extended using the available expression in the literature (Pavlović et al. 2013) up to 0.02 (BC).

$$\sigma_c = \frac{\left(k \frac{\varepsilon_c}{\varepsilon_{c1}} - \left(\frac{\varepsilon_c}{\varepsilon_{c1}}\right)^2\right) f_{cm}}{1 + (k-2) \frac{\varepsilon_c}{\varepsilon_{c1}}}, k = 1.05 E_{cm} \frac{\varepsilon_{c1}}{f_{cm}} \quad (2)$$

where σ_c is the compressive stress of the concrete, ε_c is the uniaxial strain in compression, and ε_{c1} is the strain at peak and for this concrete and equal to 0.0021. The behaviour of concrete in tension is linear up to maximum tensile strength (f_{ctm}) and then drops suddenly. Therefore, the plastic behaviour of concrete in tension is only related to its softening after reaching the maximum tensile strength. Tensile stress-strain was defined using Eq. 3, the bilinear expression provided by FIB-2010.

$$\sigma_t = \begin{cases} f_{ctm} & \varepsilon_t^{cr} = 0 \\ 0.2 f_{ctm} & \varepsilon_t^{cr} = \frac{G_f}{l_e \times f_{ctm}} \\ 0 & \varepsilon_t^{cr} = \frac{5G_f}{l_e \times f_{ctm}} \end{cases} \quad (3)$$

where σ_t is the tensile stress of the concrete, ε_t^{cr} is the cracking strain in tension, and G_f is fracture energy and equal to $73 f_{cm}^{0.18}$ (f_{cm} in MPa). The tensile plastic stress-strain of concrete (softening) is shown in Fig. 7b.

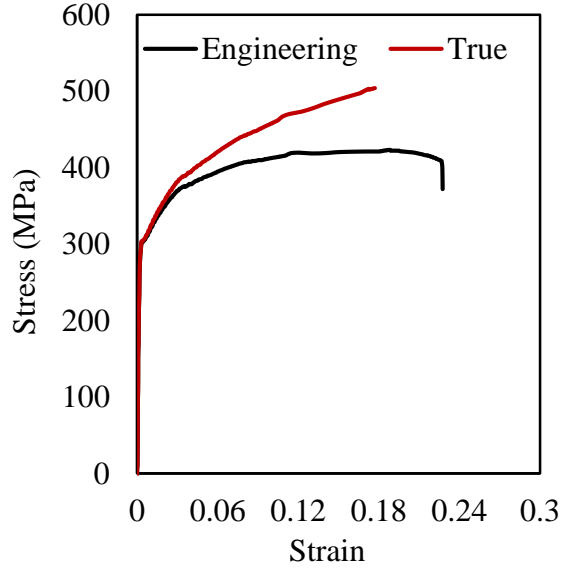


Figure 6: Engineering and true stress-strain curves.

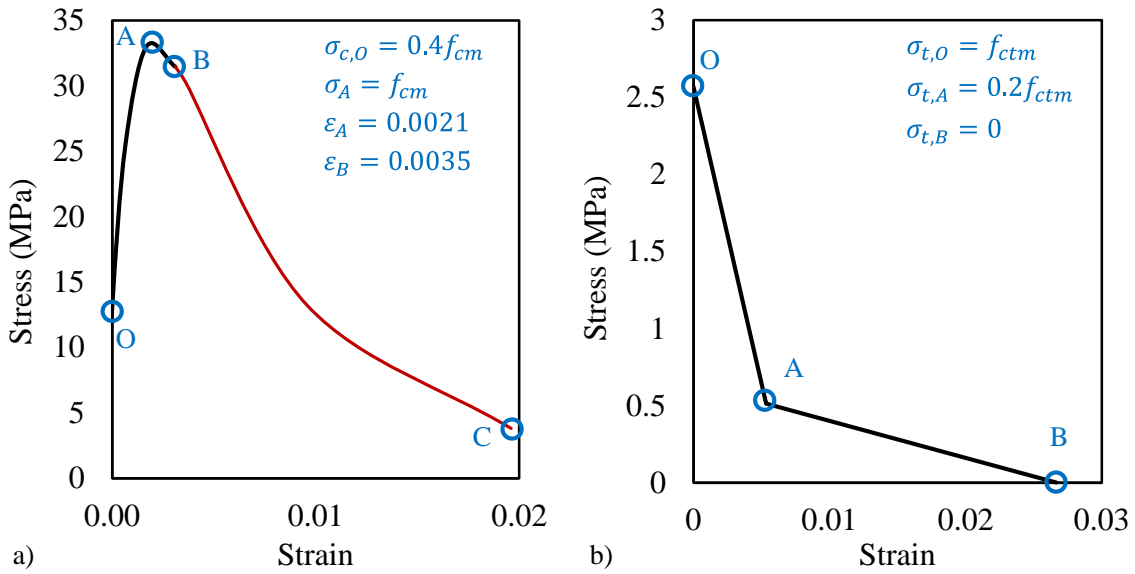


Figure 7: Concrete stress-strain curves; a) compressive and b) tensile.

The CFS profiles were modelled using a 4-node shell element (S4R element type). The 8-node solid brick element (C3D8R element type) was used to model the concrete part. The beam connector was used to model the fasteners, and the connector technique available in Abaqus defined the source and target surfaces and the fasteners' effective radius. Fig. 8 shows the details of the modelling techniques, including assembly, meshing, interaction, and boundary conditions. The reader should be aware that the tests were performed as fixed-end columns, while in the parametric study in the following section, the pin-ended boundary condition was selected to cover larger sets of columns with various slendernesses.

Initial geometric imperfection was considered for the finite element models by performing a linear buckling analysis. The first buckling model of each configuration was considered. The imperfection magnitude considered was 1/300 of the column's length based on EN 1994-1-1. For example, Fig. 9 shows the first buckling mode of the R-2C+2U short composite column.

The axial displacement loading was modelled using a dynamic explicit solver, considering the scaling factor and smooth loading amplitude. The scaling factor (Δt) was calculated considering the smallest element size (L^{el}) and material properties, including density (D_i) and modulus of elasticity (E_i), as presented in Eq. 4.

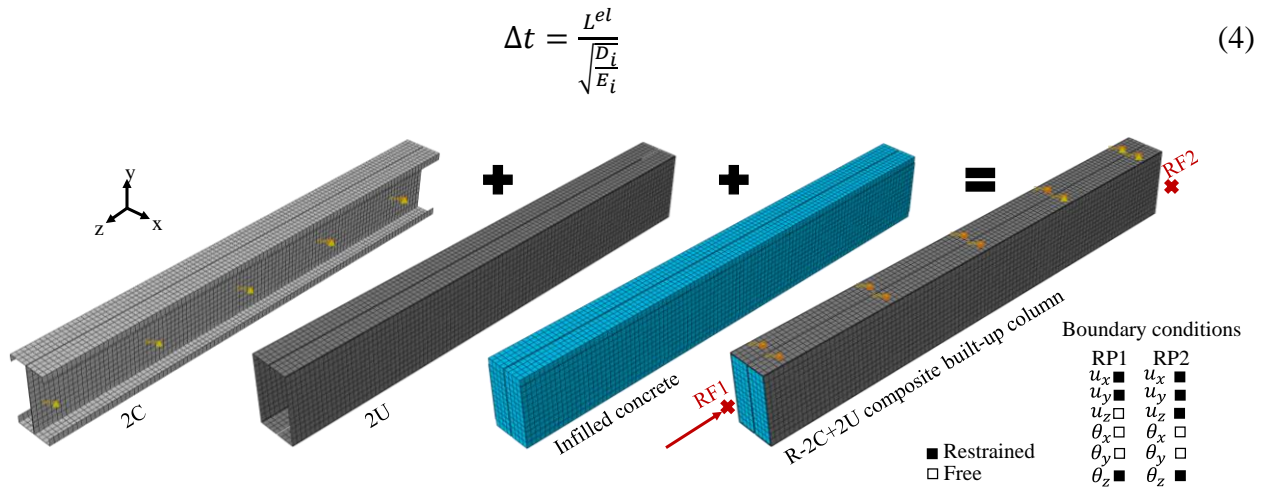


Figure 8: Finite element modelling details (example R-2C+2U short column).

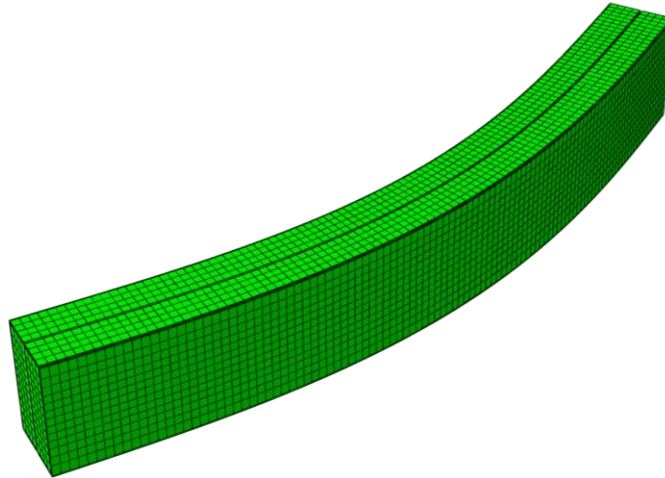


Figure 9: First buckling mode for the short CF-CFS composite column (example R-2C+2U configuration).

4. Results and discussion

4.1 Failure mode

Fig. 10 shows the buckling deformations of the experimental and numerical short CF-CFS composite columns. As can be seen, the local buckling deformation governs the failure of the

columns. The distortional and local buckling modes are visible in the plain external channels (U-shaped profiles) for all columns. According to the tests and model observation, no global buckling mode was noticed at the peak load of each short CF-CFS built-up column.

The failure mode for the long CF-CFS composite columns is shown in Fig. 11. A visible global buckling mode was detected for the rectangular configurations, as shown in Fig. 11a and Fig. 11c. However, the governed failure model for the square CF-CFS columns (S-2C+2U and S-2 Σ +2U) still was local (Fig. 11b and Fig. 11d), due to their small slenderness (<0.5).

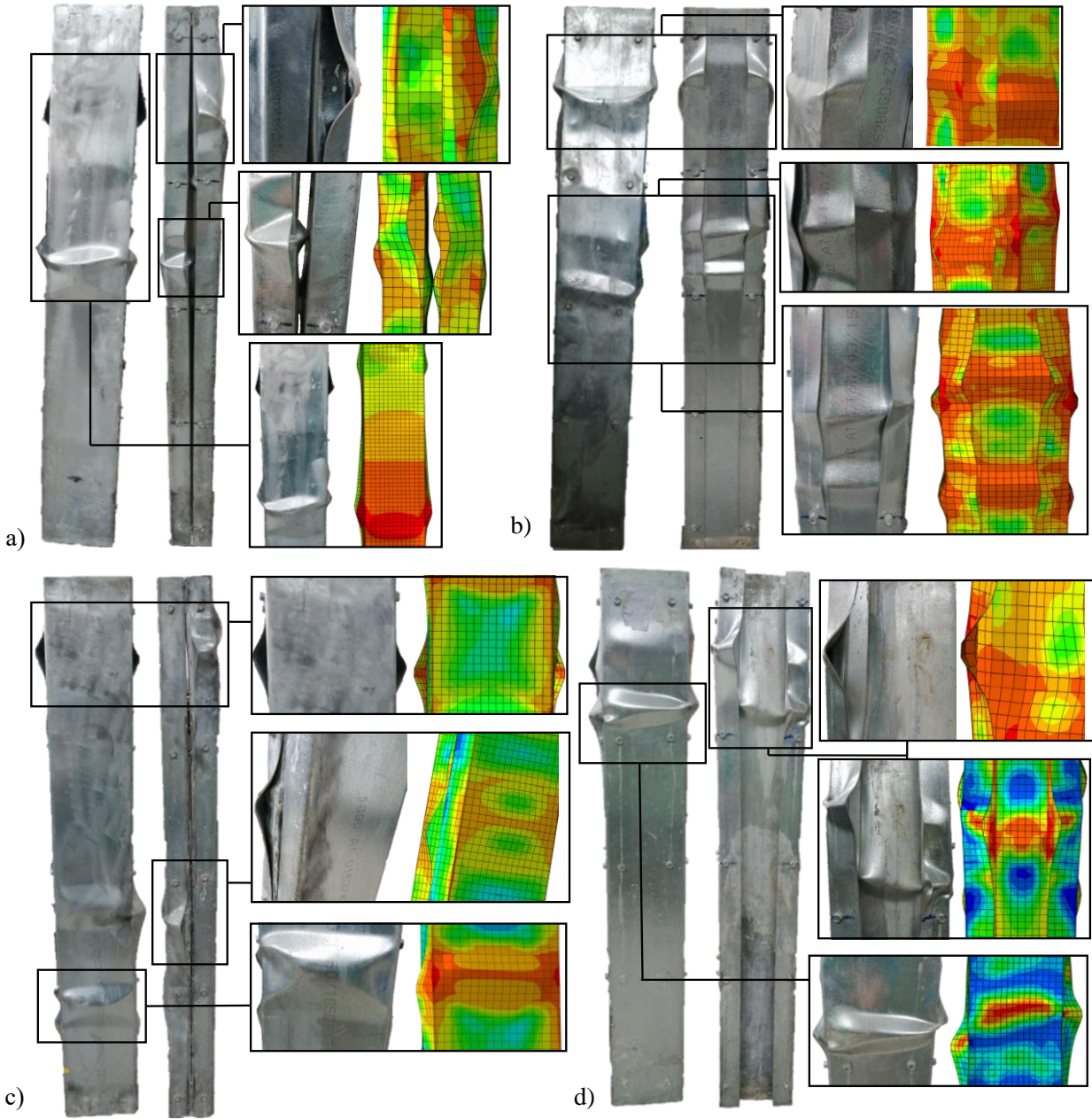


Figure 10: Comparison of failure mode of the short experimental specimens and numerical model, a) R-2C+2U, b) S-2C+2U, c) R-2 Σ +2U, and d) S-2 Σ +2U.

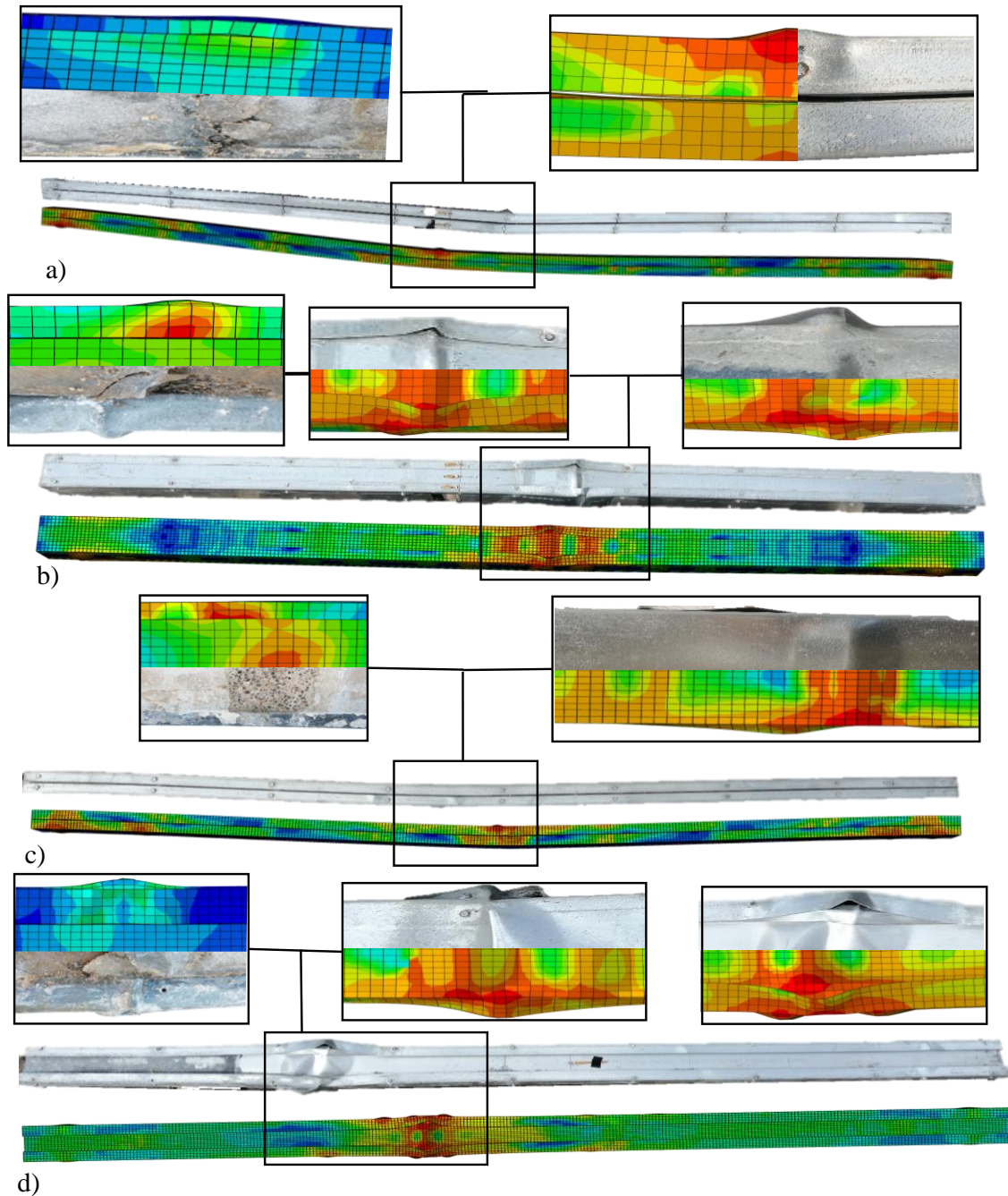


Figure 11: Comparison of buckling mode shape of the long experimental specimens and numerical models, a) R-2C+2U, b) S-2C+2U, c) R-2Σ+2U, and d) S-2Σ+2U.

4.2 Axial load-bearing capacity

Fig. 12 and Fig. 13 show the axial load vs shortening displacement for the short and long CF-CFS composite columns, respectively. Moreover, the detail of the maximum load-bearing capacity for all CF-CFS composite column specimens is listed in Table 1. A close agreement was achieved between three repetitions of each configuration with a maximum coefficient of variation (CV) of less than 5%. It can be seen that the square CF-CFS built-up configurations comprising lipped channel (C) and lipped channels with stiffened web (Σ) (S-2C+2U and S-2Σ+2U) provided greater

load-bearing capacity than the rectangular ones. This higher load-bearing capacity is mainly due to the larger concrete area.

A comparison between the obtained axial load vs shortening displacement curves from the experimental tests and numerical models was made for short (1050 mm) and long (3000 mm) CF-CFS composite columns, as depicted in Fig. 12 and Fig. 13, respectively. Moreover, a detailed comparison between the maximum load-bearing capacity of the columns obtained from the test and FEM is presented in Table 1. The results showed that the FEM results predicted the axial load-bearing capacity of the CF-CFS composite specimens with maximum differences of less than 10%.

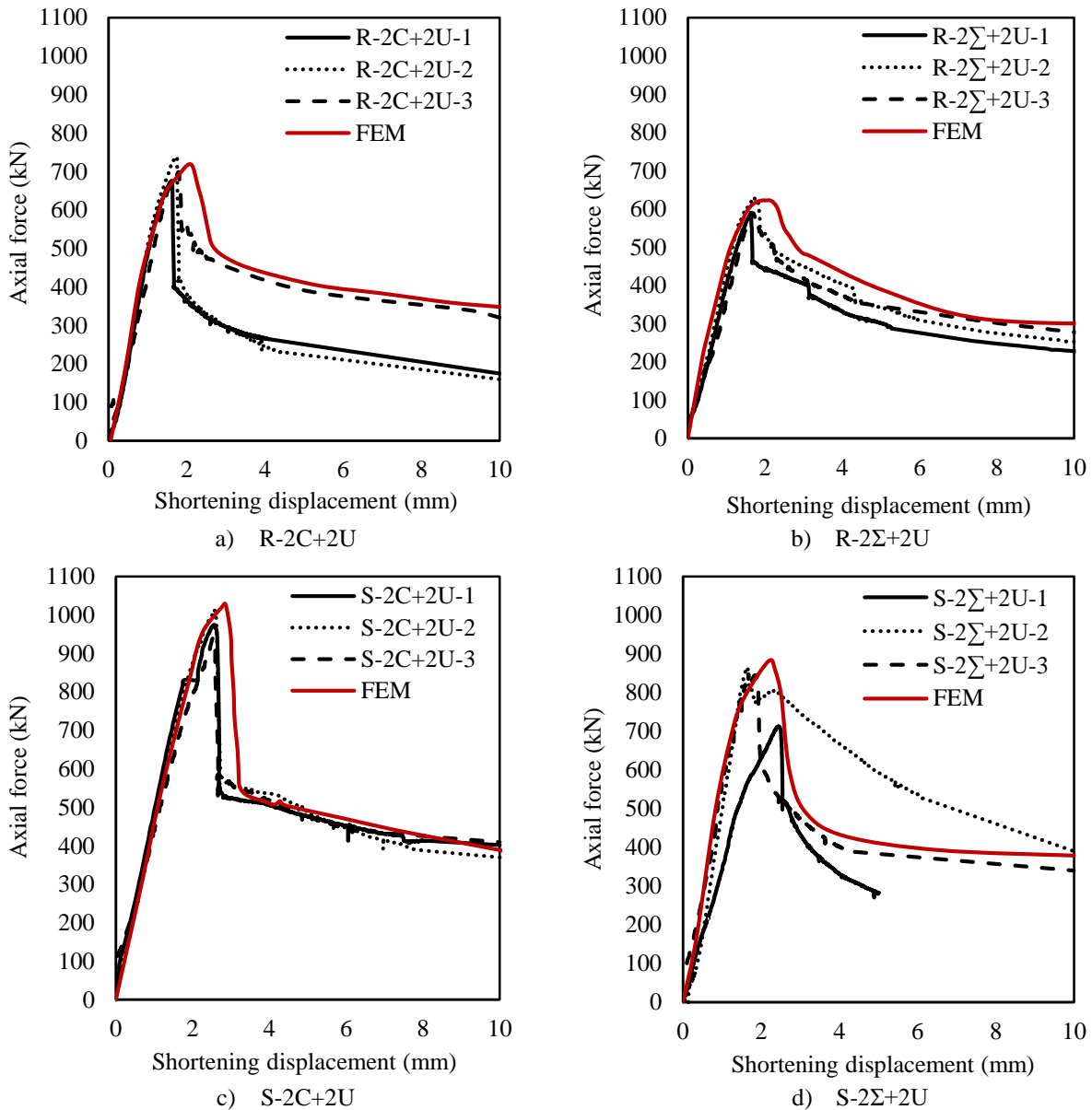


Figure 12: Axial vs shortening displacement for the short experimental specimens and numerical models.

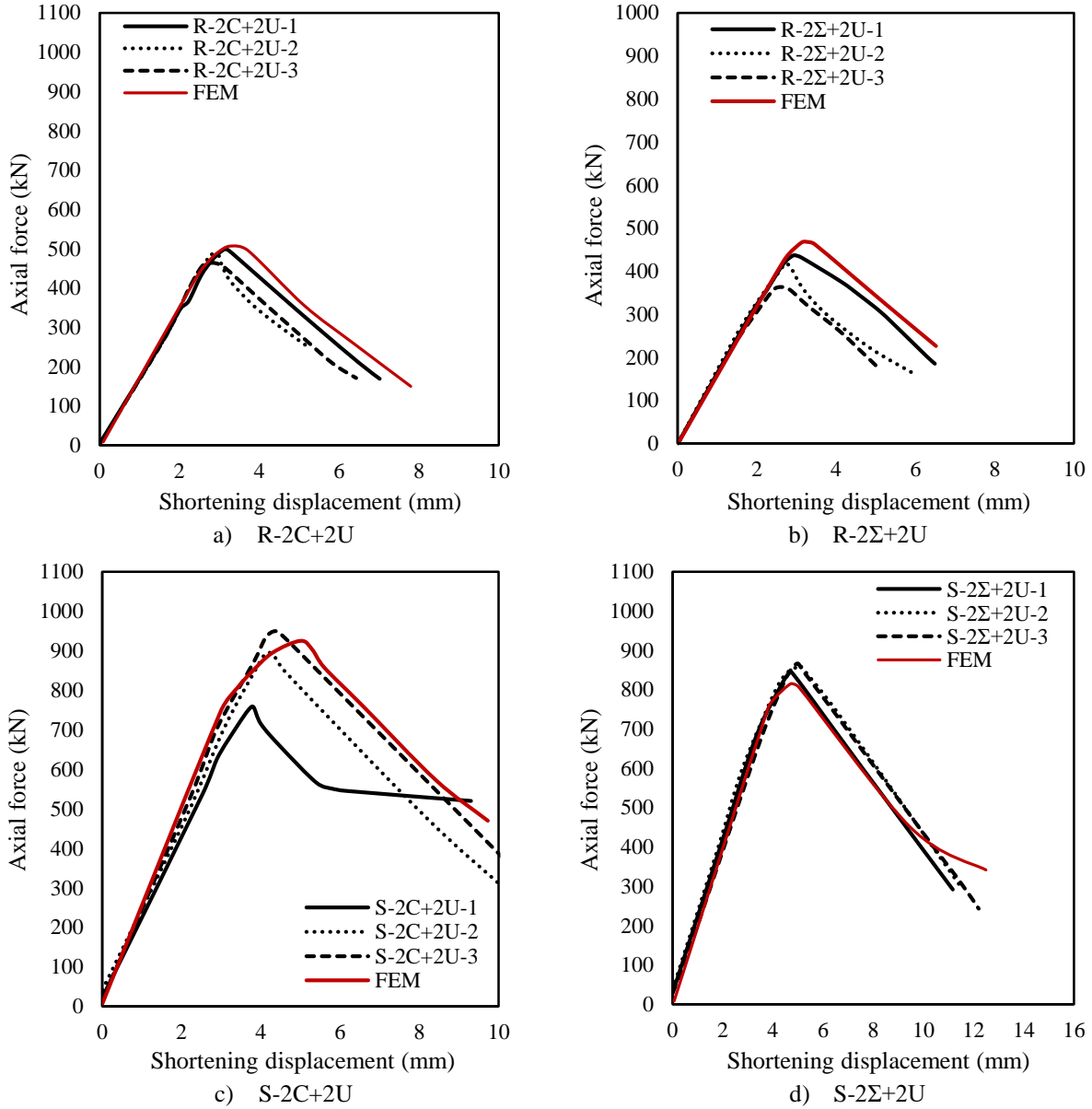


Figure 13: Axial vs shortening displacement for the long experimental specimens and numerical models.

Table 1: Comparison between the experimental tests and FEM results.

Test reference short columns (1050 mm)	$P_{u,test}$ (kN)	FEM		Test reference long columns (3000 mm)	$P_{u,test}$ (kN)	FEM	
		$N_{b,FEM}$ (kN)	$\frac{P_{b,FEM}}{P_{u,test}}$			$N_{b,FEM}$ (kN)	$\frac{P_{u,test}}{P_{b,FEM}}$
R-2C+2U-1	676.3	700.97	0.96	R-2C+2U-1	498.59	506.80	0.98
R-2C+2U-2	737.2	-	1.05	R-2C+2U-2	486.53	-	0.96
R-2C+2U-3	698.88	-	0.99	R-2C+2U-3	462.66	-	0.91
Mean value	704.12	-	1.00	Mean value	482.59	-	0.95
Standard deviation	30.78	-	0.04	Standard	18.28	-	0.03
CV (%)	4.37	-	4.37	CV (%)	3.78	-	3.78
S-2C+2U-1	974.62	1019.05	0.95	S-2C+2U-1*	757.40	921.00	0.82
S-2C+2U-2	1014.76	-	0.99	S-2C+2U-2	895.51	-	0.97

S-2C+2U-3	940.78		0.92	S-2C+2U-3	949.22		1.03
Mean value	976.72		0.95	Mean value	922.36		1.00
Standard deviation	37.03	-	0.03	Standard	37.97	-	0.10
CV (%)	3.79	-	3.79	CV (%)	4.11	-	10.72
R-2Σ+2U-1	590.26	610.27	0.96	R-2Σ+2U-1	437.5	469.50	0.93
R-2Σ+2U-2	631.27		1.03	R-2Σ+2U-2	417.45		0.88
R-2Σ+2U-3	589.38		0.96	R-2Σ+2U-3	363.25		0.77
Mean value	603.63		0.98	Mean value	427.47		0.91
Standard deviation	23.93	-	0.04	Standard	14.17	-	0.08
CV (%)	3.96	-	3.96	CV (%)	3.31	-	8.98
S-2Σ+2U-1*	712.99	858.24	0.83	S-2Σ+2U-1	844.86	815.60	1.03
S-2Σ+2U-2	866.04		1.01	S-2Σ+2U-2	862.93		1.05
S-2Σ+2U-3	847.87		0.98	S-2Σ+2U-3	865.71		1.06
Mean value	856.955		0.99	Mean value	857.83		1.05
Standard deviation	12.84	-	0.09	Standard	11.32	-	0.013
CV (%)	1.49	-	9.75	CV (%)	1.32	-	1.31
Mean value (all)			0.98	Mean value (all)			0.98
Standard deviation (all)			0.03	Standard deviation (all)			0.08
CV (%) (all)			3.71	CV (%) (all)			8.7

*Specimens with poor boundary conditions that were not considered for comparison.

4.3 Contribution of the CF-CFS components

This section investigates the contribution of the CF-CFS column components, including concrete-filled (CF) and cold-formed steel built-up columns (CFS). Moreover, the effect of concrete confinement on the CFS components was investigated by comparing the CFS contribution on the CF-CFS columns with the identical CFS built-up bare steel columns. For this purpose, the contribution of each component to the axial load-bearing capacity of the CF-CFS was obtained using the validated numerical models. Then, the axial load-bearing capacity of the CFS built-up bare steel column with identical geometry was calculated using numerical simulation.

Table 2 lists the CF and CFS contribution to the axial load-bearing capacity. Moreover, a comparison was made between the load-bearing capacity of the CFS built-up bare steel column and its contribution to the CF-CFS composite column. The results of Table 1 showed that the capacity of the CFS section significantly increased when it was used in the CF-CFS composite column. This increase is because the concrete confinement effect mitigates the early local buckling of the CFS section. However, it should be noted that for the case of the long partial CF-CFS column (R-2Σ+2U-long), no remarkable improvement in the load-bearing capacity of the CFS was seen.

Table 2: Detail of the CFS and concrete-filled contribution on the axial load-bearing capacity

Specimen	CF-CFS	CF	CFS		CFS, bare steel		
	column (kN)	contribution (kN)	%	contribution (kN)	%	column (kN)	$P_{CFS}/P_{CFS,bare}$
R-2C+2U-short	700.9	343.1	48	357.8	52	256.4	1.39
S-2C+2U-short	1019.0	672.7	66	346.3	34	245.2	1.41
R-2Σ+2U-short	610.2	244.8	40	365.4	60	328.8	1.11
S-2Σ+2U-short	858.2	499.3	58	358.9	42	322.6	1.11

R-2C+2U-long	506.8	245.4	48	261.3	52	243.1	1.07
S-2C+2U-long	921.0	602.0	65	319.0	36	236.2	1.35
R-2Σ+2U-long	469.5	165.3	35	304.2	65	302.5	1.01
S-2Σ+2U-long	815.6	445.7	55	369.9	45	333.9	1.11

5. Analytical study

5.1 Parametric study

A parametric study was performed considering an extensive range of slendernesses further to understand the behaviour of the innovative composite CF-CFS columns and investigate the applicability of available codified design methodologies, including EN 1994-1-1 and the AISC Specification. Table 3 lists the detail of the considered models. The same dimensions as the tested CF-CFS section, including the concrete area (A_c), CFS built-up cross-sectional area (A_a) were considered, while variation in column length (L) was used to generate a wide range of member slendernesses ($\bar{\lambda}$), from 0.07 to 1.49. This study used 175 finite element models (n). As for the models used for calibration purposes, the magnitude of the geometric imperfection was $L/300$. In the parametric study, all columns were pinned.

Table 3: Details of the selected models.

Configuration	n	L (mm)	$\bar{\lambda}$	A_c (mm ²)	A_a (mm ²)	$A_{a,eff}$ (mm ²)
R-2C+2U	37	250-3700	0.10-1.47	12160	1485	830
S-2C+2U	51	300-6400	0.07-1.41	8682	1518	1120
R-2Σ+2U	40	250-4000	0.93-1.49	21720	1485	830
S-2Σ+2U	47	325-6000	0.08-1.48	18333	1518	1120

5.2 Design methodology according to EN 1994-1-1

The design buckling load ($N_{b,Rd}$) for a compression member following EN 1994-1-1 is calculated using Eq. 5.

$$N_{b,Rd} = \chi N_{pl,Rd} \quad (5)$$

where χ is the reduction factor and $N_{pl,Rd}$ is the plastic resistance of the composite cross-section and is calculated using Eq.6. In Eq. 6, the effective cross-sectional area ($A_{a,eff}$) was employed because the CFS profiles are class-4 according to EN 1993-1-1.

$$N_{pl,Rd} = A_{a,eff} f_y + A_c f_{cd} \quad (6)$$

where f_y is the CFS yield stress and f_{cd} is the cylindrical compressive strength of the concrete. The reduction factor (χ) is calculated using Eqs. 7,8.

$$\chi = \frac{1}{\phi + \sqrt{\phi^2 - \bar{\lambda}^2}} \quad (7)$$

$$\phi = 0.5[1 + \alpha(\bar{\lambda} - 0.2) + \bar{\lambda}^2] \quad (8)$$

where α is the imperfection factor for the buckling curves. EN 1994-1-1 does not present a buckling curve for the CF-CFS built-up composite column; therefore, buckling curves a and b , representing the available close configurations to the current one, were selected. The imperfection factor is 0.21 for buckling curve a and 0.34 for buckling curve b . The slenderness was also calculated using Eq.9.

$$\bar{\lambda} = \sqrt{\frac{N_{pL,Rd}}{N_{cr}}}, N_{cr} = \frac{\pi^2(EI)_{eff}}{L_e^2} \quad (9)$$

where L_e is the effective length of the column and $(EI)_{eff}$ is the effective elastic flexural stiffness. The effective length of the column is the same as the column length because the pin-ended boundary condition was considered for the models.

5.3 Design methodology according to the AISC Specification

According to the AISC Specification, the design buckling load for a composite column ($N_{b,ASCE}$) can be determined using Eq. 10.

$$N_{b,AISC} = \begin{cases} P_{no}(0.658^{\frac{P_{no}}{N_{cr}}}) & \frac{P_{no}}{N_{cr}} \leq 2.25 \\ 0.877N_{cr} & \frac{P_{no}}{N_{cr}} > 2.25 \end{cases} \quad (10)$$

where P_{no} is the squash load and is obtained from Eq. 11.

$$P_{no} = \begin{cases} P_P = A_a f_y + 0.85 A_c f_{cd} & \text{For compact sections} \\ P_P - \frac{P_P - P_y}{\lambda_r - \lambda_p} (\lambda - \lambda_p)^2 & \text{For non - compact sections} \\ f_{cr} A_a + 0.7 A_c f_{cd} & \text{For slender sections} \end{cases} \quad (11)$$

where P_y is reduced squash load for noncompact sections and can be calculated using Eq. 12, and f_{cr} is critical buckling stress for slender sections and is obtained from Eq. 13. Moreover, λ , λ_r , and λ_p are the local slenderness ratios determined from Table II.1A of the AISC Specification.

$$P_y = A_a f_y + 0.7 A_c f_{cd} \quad (12)$$

$$f_{cr} = \frac{9E_s}{(D/t)^2} \quad (13)$$

where D is the depth of the CFS tube, and t is the steel tube thickness.

5.4 Reliability analysis

The reliability of the design predictions according to the EN 1994-1-1 and the AISC Specification was assessed. For this purpose, the reliability index (β) following the AISI S-100 was calculated using Eq.14.

$$\beta = \frac{\ln(M_m F_m P_m \times \frac{R_n}{Q_m})}{\sqrt{V_M^2 + V_F^2 + V_P^2 + V_Q^2}} \quad (14)$$

where M_m , F_m , V_M , and V_F are the statistical parameters assumed to be 1.10, 1.00, 0.10, and 0.05, respectively. In Eq. 14, P_m is the mean value (m) of the ratio of the buckling resistance obtained from the test or modelling over the analytical prediction, V_P is the coefficient of variation (CV), V_Q is the coefficient of the mean load effect variation and equal to 0.21 by considering $DL/LL = 0.2$. The load combination of 1.2DL+1.6LL from AISI S-100 was used to compare the results. The target reliability index of 3.0 was considered.

5.5 Results and discussion

This sub-section compares the buckling resistance of the CF-CFS built-up composite columns obtained from the finite element modelling and analytical predictions following the EN 1994-1-1 and the AISC Specification. Fig. 14 compares the FE buckling resistance over the plastic resistance ratio ($N_{b,FEM}/N_{pl,Rd}$) with the available buckling curves (a and b) from EN 1993-1-1 for all CF-CFS configurations. As can be seen, the buckling curve- a does not sufficiently predict the reduction factor obtained from the models, especially for a slenderness value higher than 0.5. Moreover, the buckling curve b is highly conservative for a slenderness value lower than 0.67. Additionally, buckling curve b does not predict the reduction factor obtained from the models for the case of R-2 Σ +2U.

Fig. 15 compares the buckling resistance obtained from the numerical simulations and analytical predictions from the EN 1994-1-1 for all configurations with various slendernesses. As can be seen, the design considering buckling curve a does not sufficiently predict the buckling resistance of the CF-CFS columns with various slendernesses. For the case of R-2C+2U, the buckling resistance prediction for the columns with non-dimensional slenderness between 0.67-1.36 was unconservative, while the design prediction considering buckling curve b was highly conservative with a mean $N_{b,FEM}/N_{b,Rd}$ ratio of 1.24. A similar conclusion can be made for the other full concrete-filled CFS columns (S-2C+2U and S-2 Σ +2U). The reliability index of the design prediction according to EN 1994-1-1 considering buckling curve b for the concrete-filled CFS columns (R-2C+2U, S-2C+2U and S-2 Σ +2U) was higher than 3. However, this high-reliability index was expected since the design predictions were very conservative.

For the partial concrete filled configuration (R-2 Σ +2U), the design according to EN 1994-1-1, considering both buckling curves a and b , was unconservative. The reliability indexes were 1.94 and 2.69 for the design prediction considering buckling curves a and b , respectively.

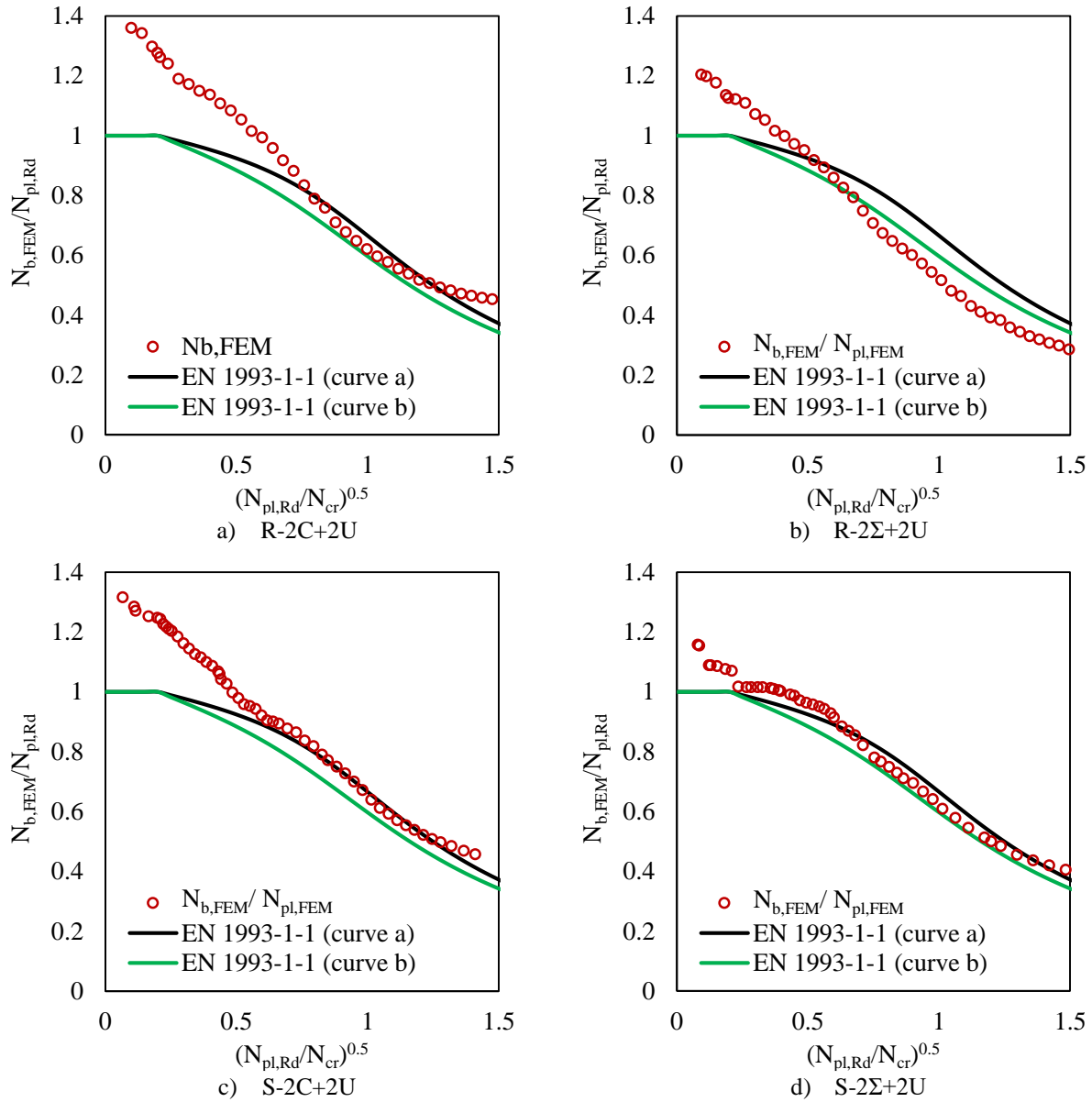


Figure 14: Comparison between buckling curves and reduction from the FEM.

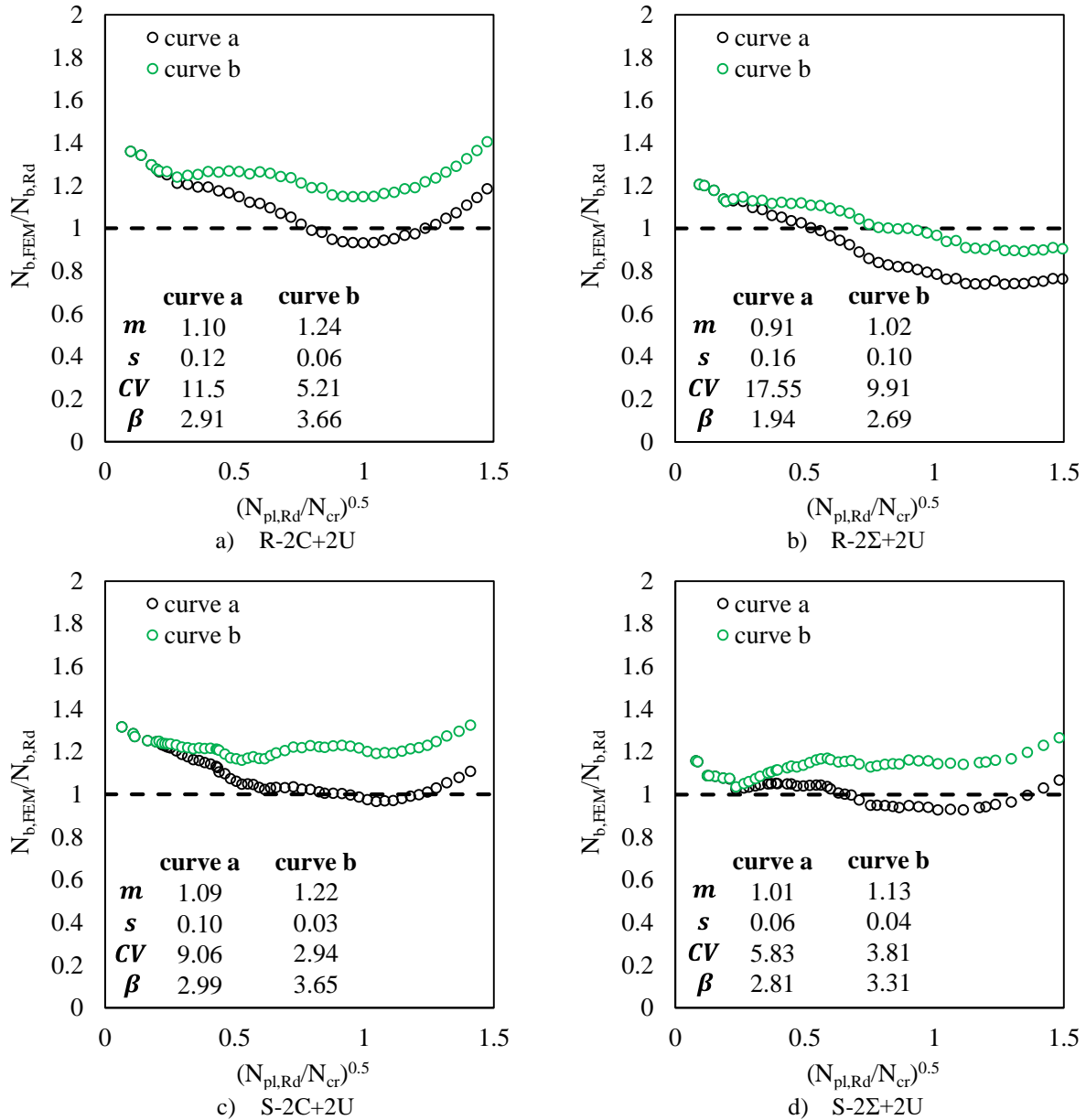


Figure 15: Comparison between buckling resistance obtained from the FEM and EN 1994-1-1.

This section also assesses the applicability of the AISC Specification to predict the axial load-bearing capacity of the innovative CF-CFS columns. However, the AISC Specification does not present a clear strategy to determine the thickness of the CFS built-up sections used as a composite column component. Therefore, this study investigated the applicability of the AISC Specification by considering two thicknesses, including a) thickness of the single CFS profile and b) the equivalent thickness for the built-up section (t_{eq}).

Fig. 16 shows the strategy to calculate the equivalent thickness (t_{eq}) of the built-up section (example for S-2C+2U section). The equivalent thickness was calculated by weighting the overlapped (t_{eq}) and single (t) CFS plates (see Fig. 16).

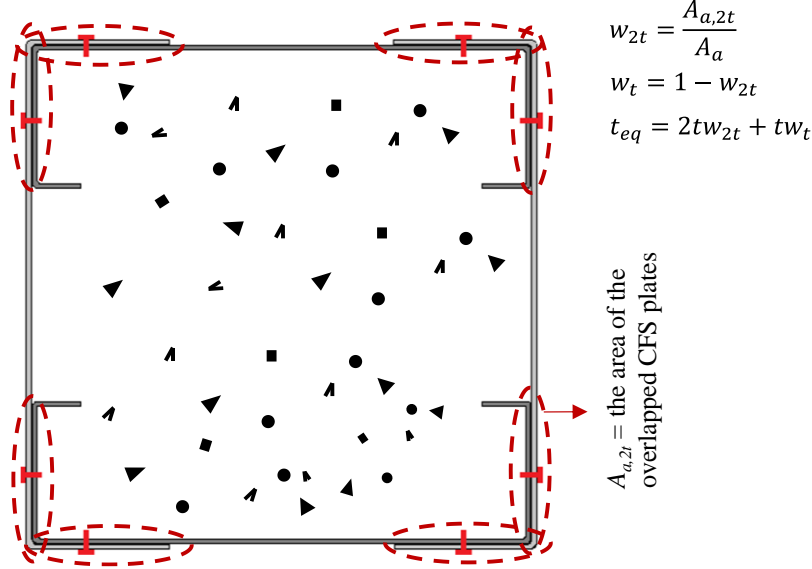


Figure 16: Calculation of the equivalent thickness (t_{eq}).

A comparison between the buckling resistance prediction according to the AISC Specification and those obtained numerically was made for all configurations, as shown in Fig. 17. As shown, the design prediction according to the AISC Specification is highly conservative for the full CF composite columns (R-2C+2U, S-2C+2U, and S-2Σ+2U), when single CFS thickness was considered as the thickness of the built-up section. The mean $N_{b,FEM} / N_{b,AISC}$ ratio was obtained as 1.24, 1.32, and 1.29 for R-2C+2U, S-2C+2U, and S-2Σ+2U, respectively. The reliability index of the AISC Specification to predict the buckling resistance of full CF-CFS composite columns (R-2C+2U, S-2C+2U, and S-2Σ+2U) was higher than 3; however, this high-reliability index is due to the high conservative prediction.

By comparing the results, it was found that the accuracy of the buckling resistance of the full CF-CFS columns was increased by using the equivalent thickness of the CFS built-up instead of a single profile thickness. As can be seen, by using the proposed equivalent thickness, the $N_{b,FEM} / N_{b,AISC}$ ratio was obtained as 1.05, 1.01, and 1.04 with a maximum CV of 2.89% for the R-2C+2U, S-2C+2U, and S-2Σ+2U. However, the analytical prediction according to the AISC Specification by considering the proposed equivalent thicknesses did not reasonably predict the buckling resistance of the partial CF-CFS composite column (R-2Σ+2U). It is due to the existence of an inner void; therefore, more investigation is needed to address this issue and propose a suitable modification for this kind of double-skin partial concrete-filled columns.

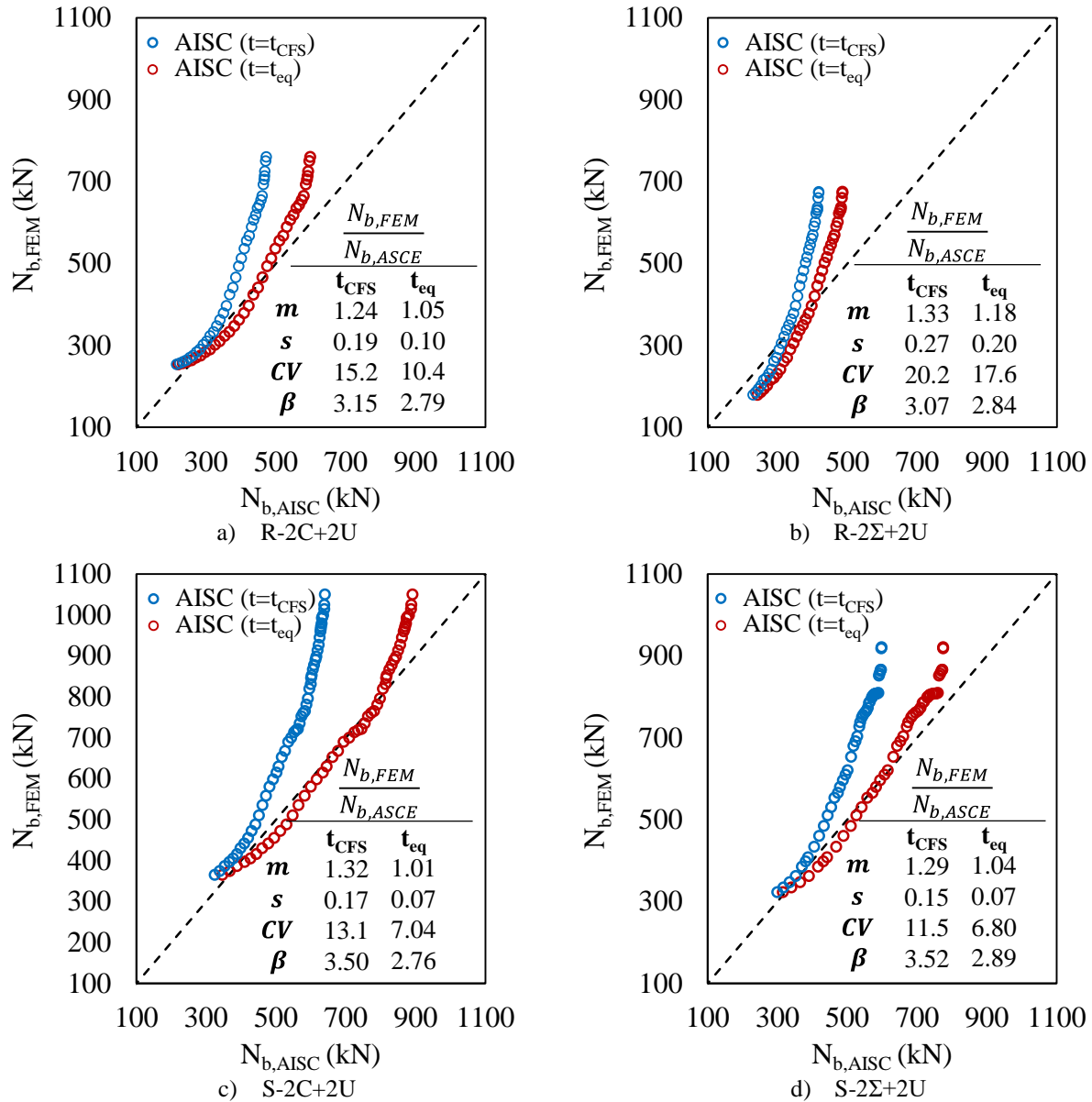


Figure 17: Comparison between buckling resistance obtained from the FEM and the AISC Specification.

6. Proposed buckling curves for the EN 1994-1-1

This section discusses and proposes new buckling curves to design buckling resistance of full and partial CF-CFS composite columns following the EN 1994-1-1 procedure. The FEM buckling resistance over the plastic resistance ratio ($N_{b,FEM}/N_{pl,Rd}$) and the failure modes for all CF-CFS configurations are shown in Fig 18. As also Fig. 14, the buckling curves suggested by EN 1994-1-1 do not present a reduction factor up to the non-dimensional slenderness of 0.2. However, the results of Fig. 18 show that this range of non-dimensional slenderness can be extended to 0.4. Moreover, Fig. 18 shows that the failure mode for square and rectangular CF-CFS composite columns is pure local up to non-dimensional slenderness of 0.4, while for the CF-CFS columns with non-dimensional slenderness higher than 0.4, the failure mode is an interaction of global

flexural and local. Therefore, Eq. 8 was modified for the CF-CFS composite columns by extending the unreduced range of the buckling curve to 0.4, as presented in Eq.15.

$$\Phi = 0.5[1 + 0.39(\bar{\lambda} - 0.4) + \bar{\lambda}^2] \quad (15)$$

where the imperfection factor is proposed to be 0.39 for full CF-CFS composite columns (curve *e*) and 0.79 for partial CF-CFS composite columns (curve *f*).

Fig. 19 compares the buckling resistance obtained from the numerical simulation and analytical predictions from EN 1994-1-1, considering the proposed buckling curves *e* and *f*. As can be seen, the EN 1994-1-1, considering the proposed buckling curves *e* and *f*, accurately predicted the buckling resistance of the CF-CFS composite columns with different slendernesses. The ratio of $N_{b,FEM}/N_{pl,Rd}$ obtained as 1.08 with CV = 8% and reliability index of 3.00 for full CF-CFS (R-2C+2U, S-2C+2U, and S-2Σ+2U), and 1.05 with CV = 5.8% and reliability index of 2.96 for partial CF-CFS (R-2Σ+2U) composite columns.

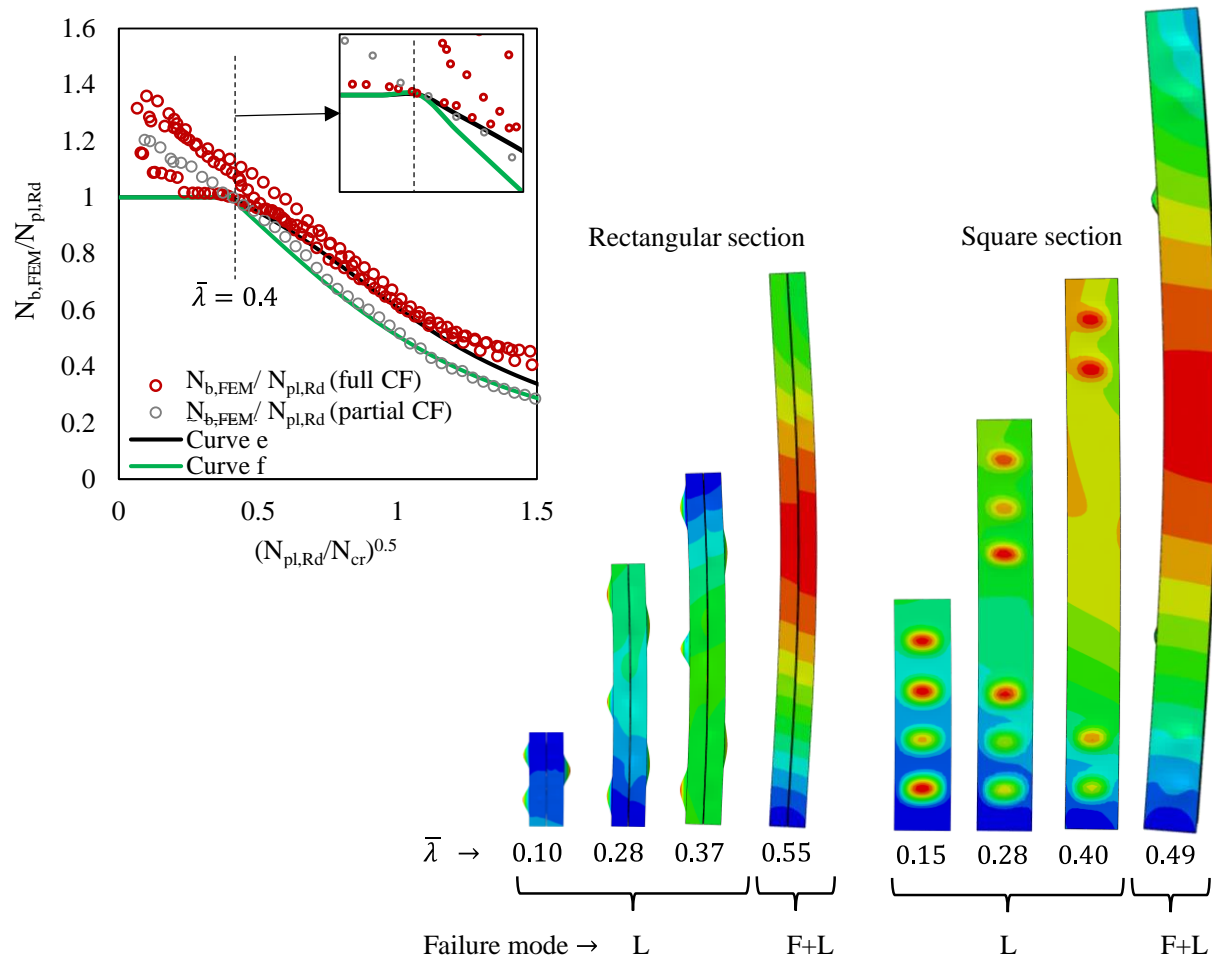


Figure 18: Proposed curves and the failure modes.

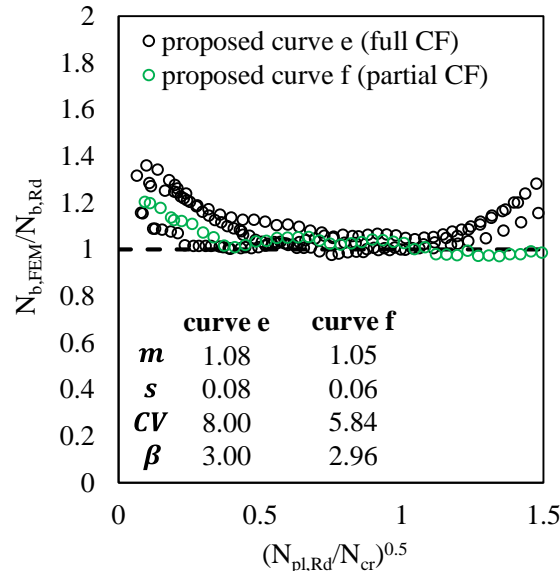


Figure 19: Comparison between buckling resistance obtained from the FEM and proposed buckling curves.

7. Conclusions

An innovative full and partial concrete-filled cold-formed steel (CF-CFS) built-up composite column has been introduced. The buckling resistance of the short and slender rectangular and square CF-CFS composite columns has been studied. First, tests on short and slender CF-CFS composite column was carried out. The finite element modelling approach was then developed and validated against the test results. Finally, parametric studies were conducted using the validated modelling technique, addressing the effect of the CF-CFS slenderness. The results were compared with buckling resistance prediction according to EN 1994-1-1 and the AISC Specification to assess their applicability for designing CF-CFS columns.

The applicability of EN 1994-1-1 was assessed by considering buckling curves *a* and *b*, resulting in an unconservative prediction for all configurations considering buckling curve *a*, especially for CF-CFS with intermediate slenderness, and highly conservative prediction by considering buckling curve *b*. However, the EN 1994-1-1 prediction for the partial CF-CFS composite column was unconservative considering both curves *a* and *b*. Similarly, the applicability of the AISC Specification was assessed. The AISC methodology for concrete-filled steel tube columns highly relies on steel tube thickness. However, no guideline has been proposed for the CFS built-up sections. Therefore, the buckling resistance of CF-CFS was predicted by considering two strategies for determining the steel tube thickness, including the thickness of a single CFS profile and the equivalent thickness of the CFS built-up section. The results showed that the buckling resistance according to the AISC Specification by considering single profile thickness is highly conservative, while more accurate results were achieved considering the equivalent thickness.

Attention was finally given to the behaviour of CF-CFS columns to determine the more accurate non-dimensional slenderness that determines the limit between short and slender CF-CFS columns. Again, the FE models were shown to accurately capture the load-deformation response and failure modes of the tests. After examining the structural behaviour of the CF-CFS columns, the unreduced constant range of recommended buckling curves of EN 1994-1-1 was then extended

from non-dimensional slenderness of 0.2 to 0.4. Finally, buckling curves were explicitly proposed for the partial and full CF-CFS to predict their buckling resistance with high accuracy.

Acknowledgements

This work is financed by national funds through Foundation for Science and Technology (FCT), under grant agreement 2021.06528.BD attributed to the 1st author and under the grant agreement 2020.03588.CEECIND attributed to the 2nd author.

The authors gratefully acknowledge the Portuguese Foundation for Science and Technology (FCT) for its support under the framework of the research project PTDC/ECI-EGC/31858/2017 – INNOCFSCONC – Innovative hybrid structural solutions using cold-formed steel and lightweight concrete”, financed by FEDER funds through the Competitiveness Operational Programme – COMPETE and by national funds through FCT and D_INNOCFSCONC – “Demonstração de Solução Estrutural Híbrida Inovadora com Recurso a Aço-Enformado a Frio e Betão Leve”, funded by the call for starting projects and proof of concept projects UI-Transfer, with operation Code POCI-01-0246-FEDER-181315 financed by COMPETE 2020.

This work was partly financed by FCT/MCTES through national funds (PIDDAC) under the R&D Unit Institute for Sustainability and Innovation in Structural Engineering (ISISE), under reference UIDB/04029/2020.

References

- Rahnavard, R., Craveiro, H.D., Simões, R.A., Laím, L., Santiago, A. (2022). “Buckling resistance of concrete-filled cold-formed steel (CF-CFS) built-up short columns under compression.” *Thin-Walled Structures*, Volume 170, 108638.
- Rahnavard, R., Craveiro, H.D., Simões, R.A. (2022). “Innovative concrete-filled cold-formed steel (CF-CFS) built-up columns.” *Cold-Formed Steel Research Consortium Colloquium*, USA.
- Rahnavard, R., Craveiro, H.D., Lopes, M., Simões, R.A., Laím, L., Rebelo, C. (2022). “Concrete-filled cold-formed steel (CF-CFS) built-up columns under compression: test and design.” *Thin-Walled Structures*. Volume 179, 109603
- Han, L.H., Ren, Q.X., Li, W. (2011). “Tests on stub stainless steel–concrete–carbon steel double-skin tubular (DST) columns.” *Journal of Constructional Steel Research*, Volume 67, Issue 3, Pages 437-452.
- Uy, B. Tao, Z., Han, L.H., (2011). “Behaviour of short and slender concrete-filled stainless steel tubular columns.” *Journal of Constructional Steel Research*, Volume 67, Issue 3, Pages 360-378.
- Hassanein, M.F., Kharoob, O.F., Gardner, L. (2014). “Analysis of circular concrete-filled double skin tubular slender columns with external stainless steel tubes.” *Thin-Walled Structures*, Volume 79, Pages 23-37.
- Hassanein, M.F., Kharoob, O.F., Gardner, L. (2015). “Behaviour and design of square concrete-filled double skin tubular columns with inner circular tubes.” *Engineering Structures*, Volume 100, 2015, Pages 410-424.
- Kazemzadeh A. S, Uy, B. (2020). “Effect of concrete infill on local buckling capacity of circular tubes.” *Journal of Constructional Steel Research*, Volume 165, 105899.
- Hassanein, M.F., Silvestre, N., Yan, X.F. (2023). “Confinement-based direct design of circular concrete-filled double-skin normal and high strength steel short columns.” *Thin-Walled Structures*, Volume 183, 110446.
- Uenaka, K., Kitoh, H., Sonoda, K. (2010). “Concrete filled double skin circular stub columns under compression.” *Thin-Walled Structures*, Volume 48, Issue 1, Pages 19-24.
- Yan, X.F., Zhao, Y.G., Lin, S., Zhang, H. (2021). “Confining stress path-based compressive strength model of axially compressed circular concrete-filled double-skin steel tubular short columns.” *Thin-Walled Structures*, Volume 165, 107949.
- EN 1994-1-1 (2004). Eurocode 4: Design of Composite Steel and Concrete Structures, Part 1.1: General Rules and Rules for Building.
- AISC 360. (2010). Load and resistance factor design specification for structural steel buildings. American Institute of Steel Construction, Chicago.

Craveiro, D.H., Rahnavard, R. Laím, L., Simões, R.A., Santiago, A. (2022). "Buckling behavior of closed built-up cold-formed steel columns under compression." *Thin-Walled Structures*, Volume 179, 109493.

Abaqus Analysis User's Guide. (2017), Version 6.17 Dassault Systèmes Simulia USA.

EN 1992-1-1 (2004): Eurocode 2: Design of concrete structures - Part 1-1: General rules and rules for buildings.

Pavlović, M., Marković, Z., Veljković, M., Buđevac, D. (2013). "Bolted shear connectors vs. headed studs behaviour in push-out tests." *Journal of Constructional Steel Research*, Volume 88, Page 134-149.

Fib Model Code for Concrete Structures, (2010).

EN 1993-1-1 (2005) Eurocode 3: Design of steel structures - Part 1-1: General rules and rules for buildings.

AISI S100-16. (2016). North American Specification for the Design of Cold-Formed Steel Structural Members. Washington, DC, U.S.A.